

Directed growth of single-crystal indium wires

Ishan Talukdar, Birol Ozturk, Bret N. Flanders, and Tetsuya D. Mishima

Citation: [Applied Physics Letters](#) **88**, 221907 (2006); doi: 10.1063/1.2208431

View online: <http://dx.doi.org/10.1063/1.2208431>

View Table of Contents: <http://scitation.aip.org/content/aip/journal/apl/88/22?ver=pdfcov>

Published by the [AIP Publishing](#)

Articles you may be interested in

[Constrained, aqueous growth of three-dimensional single crystalline zinc oxide structures](#)

APL Mat. **2**, 012111 (2014); 10.1063/1.4863075

[Ferroelectric properties and dynamic scaling of 100 oriented \(K 0.5 Na 0.5 \) NbO 3 single crystals](#)

Appl. Phys. Lett. **98**, 242906 (2011); 10.1063/1.3600058

[Facile hydrothermal preparation and characterizations of single crystalline Ge dioxide nanowires](#)

J. Appl. Phys. **105**, 054313 (2009); 10.1063/1.3078819

[In situ growth of aligned CdS nanowire arrays on Cd foil and their optical and electron field emission properties](#)

J. Appl. Phys. **104**, 014312 (2008); 10.1063/1.2952013

[Self-catalytic solution for single-crystal nanowire and nanotube growth](#)

J. Chem. Phys. **127**, 244702 (2007); 10.1063/1.2813432

The advertisement features a red and white color scheme. On the left, text reads 'Confidently measure down to 0.01 fA and up to 10 PΩ' and 'KeySight B2980A Series Picoammeters/Electrometers'. Below this is a red button with the text 'View video demo'. On the right, there is an image of the KeySight B2980A device and the KeySight Technologies logo.

Directed growth of single-crystal indium wires

Ishan Talukdar, Birol Ozturk, and Bret N. Flanders^{a)}

Department of Physics, Oklahoma State University, Stillwater, Oklahoma 74078

Tetsuya D. Mishima

Homer L. Dodge Department of Physics and Astronomy, University of Oklahoma, Norman, Oklahoma 73019

(Received 24 November 2005; accepted 12 April 2006; published online 31 May 2006)

Tailored electric fields were used to direct the dendritic growth of crystalline indium wires between lithographic electrodes immersed in solutions of indium acetate. Determination of the conditions that suppress sidebranching on these structures has enabled the fabrication of arbitrarily long needle-shaped wires with diameters as small as 370 nm. Electron diffraction studies indicate that these wires are crystalline indium, that the unbranched wire segments are single-crystal domains, and that the predominant growth direction is near $\langle 110 \rangle$. This work constitutes a critical step towards the use of simply prepared aqueous mixtures as a convenient means of controlling the composition of submicron, crystalline wires. © 2006 American Institute of Physics. [DOI: 10.1063/1.2208431]

Directed wire-growth techniques enable the one-step assembly and interfacing of submicron interconnects composed of a wide variety of materials^{1–4} and, therefore, are promising approaches to the fabrication of high quality photonic, mechanical, and electronic devices. To realize these goals, precise control over the structure of the wires is necessary, as their structural properties will dictate their optical, mechanical, and electronic properties in device applications. Recent studies have revealed the potential of dielectrophoresis for attaining impressive structural control over assembled wires. In a solution-phase study, Kretschmer and Fritzsche, produced wires composed of 30-nm-diameter gold nanoparticles that were arranged in a pearl-necklace configuration;⁵ this outcome demonstrates the assembly of interconnects with *mesoscopic* structural precision, where the organization of the particles composing the wire is periodic. In a separate, gas-phase study, Libbrecht and Tanusheva used dielectrophoretic forces to direct the growth of ice crystals;⁶ this work demonstrates the growth of dendrites with *microscopic* structural precision, where the organization of the molecules composing the dendrite is periodic. Attaining such *microstructural* control in solution-phase directed assembly would provide a straightforward means of growing high quality wires of composition determined simply by choice of solute. To this end, Cheng *et al.* have fabricated wires from simple, aqueous solutions of palladium acetate.⁷ While this work stopped short of determining the stoichiometric composition or crystallinity of the wires, it demonstrated directed wire growth in solutions containing only dissolved salt. The present work builds on these previous studies to demonstrate methodology for the electrochemical growth of single crystal indium wires from aqueous solutions of indium acetate. This work demonstrates the use of a simple salt solution as a medium in which to grow single-crystal metal wires between targeted sites in a circuit.

Figure 1 shows a diagram of the wire-growth apparatus. The function generator (Hewlett Packard, 8111A) supplies an alternating voltage that is passed through an amplifier (FLC

Electronics, F10A) and applied across the lithographic electrodes. These electrodes are deposited on 1-mm-thick Pyrex substrates, using standard lithographic techniques, as described elsewhere.⁸ The optical micrograph in Fig. 1 depicts the ends of a tapered electrode pair. The wire spanning the 60 μm electrode gap was grown by depositing a 10 μl drop of a 0.055M aqueous solution of indium acetate [$\text{In}(\text{CH}_3\text{COO})_3$] over the gap and applying a 1.0 MHz square wave with an amplitude of 18 V and no dc offset. The wire grew from the alternating electrode to the grounded electrode immediately (to the eye) after switching on the alternating voltage. When the wire interfaced with the opposing electrode, the voltage was terminated manually. The growth process was observed on an inverted microscope (Leica, IRB) equipped with a digital camera (Roper, CoolSnap).

For a given electrode gap and geometry, variation of the voltage amplitude, its frequency, and the $\text{In}(\text{CH}_3\text{COO})_3$ concentration gives rise to a wide range of wire structures. Figure 2(a) depicts a concentration-voltage phase diagram of interconnect structural types, all of which were fabricated between electrodes spaced by 60 μm , with an ac frequency of 1.0 MHz. When the voltage amplitude was less than 18 V, interconnect formation did not occur, regardless of the $\text{In}(\text{CH}_3\text{COO})_3$ concentration. For concentrations less than

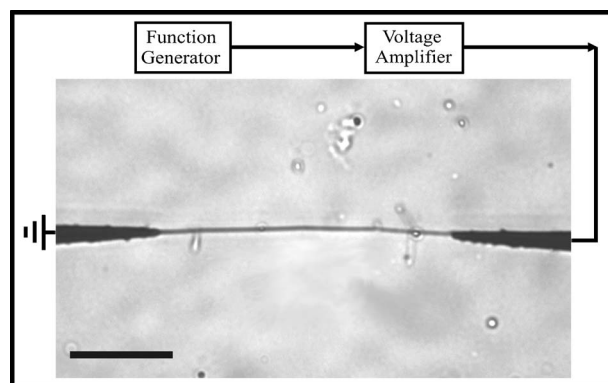


FIG. 1. Apparatus for directed electrochemical wire growth. The image is an optical micrograph of a wire grown from indium acetate solution. The scale bar denotes 20 μm .

^{a)} Author to whom correspondence should be addressed; electronic mail: bret.flanders@okstate.edu

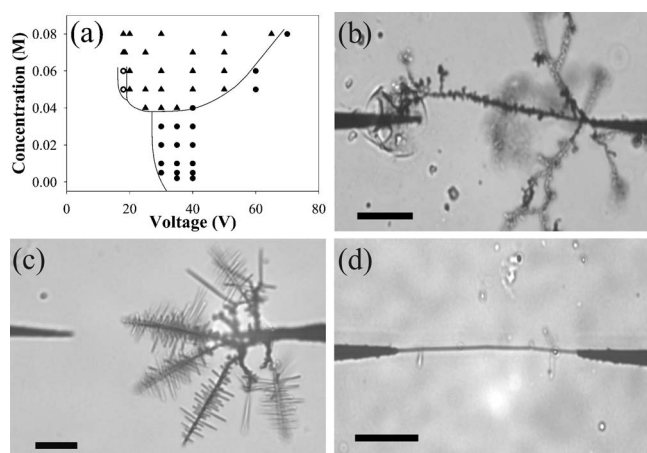


FIG. 2. (a) Concentration-voltage phase diagram of interconnect types. The conditions that give rise to amorphous, dendritic and needle-shaped wires are denoted by the filled circles, the filled triangles, and the unfilled circles, respectively. (b) A representative image of an amorphous wire. (c) A representative image of a dendritic structure. (d) A representative image of a needle-shaped wire. The scale bars in images (b)–(d) represent $20\ \mu\text{m}$.

$0.040M$ and voltages greater than $30\ \text{V}$, wires with an amorphous appearance spontaneously grew. The filled circles denote this region in Fig. 2(a) and 2(b) depicts a typical amorphous wire. Increasing the $\text{In}(\text{CH}_3\text{COO})_3$ concentration to greater than $0.040M$ caused dendritic wire growth. The filled triangles denote this region in Fig. 2(a) and 2(c) depicts a typical dendritic sample. A real-time movie of this dendritic growth process is available as supplementary material (see Ref. 19). Setting the voltage to $18\ \text{V}$ and using a saturated ($0.055M$) indium acetate solution gives rise to suppressed sidebranching and the formation of individual, needle-shaped wires. The unfilled circles denote this small region of phase space in Fig. 2(a) and 2(d) depicts a representative wire. A real-time movie of the needle-growth process is available as supplementary material (see Ref. 19). The dendritic wires presented here are similar in appearance to the dendritic structures that were previously observed in ZnSO_4 solutions;^{9,10} however, in the present case, their growth is directed.

A $200\ \text{kV}$ transmission electron microscope (TEM) made by JEOL (JEM-2000FX) was used to obtain detailed crystallographic information of the dendritic wires. Because the pyrex substrates of the electrode arrays are not thin enough to transmit the electron beam, it was necessary to transfer the wires to TEM grids. The transfer process consisted of using an actuator to push a holey carbon grid (Ted Pella) across the wire-laden electrode gap. To increase the

probability of successful transfer, we populated the liquid in the interelectrode region with several wire segments, breaking each wire free of the electrode after its growth. Translating the TEM grid through this dispersion caused the wires to flow onto the grid. Figure 3(a) shows a TEM micrograph of a group of wires that were mounted in this manner. The wires are needle shaped with sparse side branching. The six wires depicted in this image range in diameters from 367 to $556\ \text{nm}$.

Figure 3(b) depicts a selected area electron diffraction pattern collected from the wire segment indicated by the arrow and oriented as shown in Fig. 3(a). Because the area selected by the $\sim 1\text{-}\mu\text{m}$ -diameter aperture did not include any portion of the carbon grid, no ring patterns due to amorphous carbon are evident in this figure. Figure 3(c) shows a simulated $[111]$ diffraction pattern that was calculated using a commercial software package (Virtual Laboratories, Desktop Microscopist), requiring as input the camera length ($790.8\ \text{mm}$), the electron wavelength ($2.51 \times 10^{-3}\ \text{nm}$), and the known structural parameters of crystalline indium: a tetragonal crystal structure, with $a=b=0.3251\ \text{nm}$ and $c=0.4945\ \text{nm}$, belonging to symmetry group $I4/mmm$.¹¹ The experimental and simulated diffraction patterns are in excellent quantitative agreement with each other. For example, on the TEM film the distances of the $01\bar{1}$ and $\bar{1}10$ spots from the 000 spot are 7.33 and $8.57\ \text{mm}$, respectively; the angle subtended by these diffracted spots is $53.7^\circ \pm 0.4^\circ$. The corresponding calculated values are $7.31\ \text{mm}$, $8.64\ \text{mm}$, and 53.78° . The error for each of these quantities is less than 0.85% . This close agreement indicates that the wire is composed of crystalline indium. Of 13 wires examined in this manner, all were crystalline indium.

To determine the continuity of the crystalline regions of these wires, selected area diffraction patterns were collected from successive positions along their lengths, using an area selection aperture with a $2.2\ \mu\text{m}$ diameter. Figures 4(a)–4(c) represent diffraction patterns captured from the lower, middle, and upper sections of the $\sim 5\text{-}\mu\text{m}$ -long wire indicated in Fig. 3(a). For this measurement, the sample was rotated so that the electron beam impinged upon a different face of the wire. Analyses of the discrete patterns in Figs. 4(a)–4(c) indicate that all three diffraction patterns result from crystalline indium observed from the $\langle 001 \rangle$ direction, confirming the structural assignment made above. The diffuse rings in these images result from the amorphous carbon strands of the TEM grid beneath the wire segment. Moreover, in each of the three images, the $\langle 001 \rangle$ diffraction pattern is identically oriented, the diffracted spots are located the

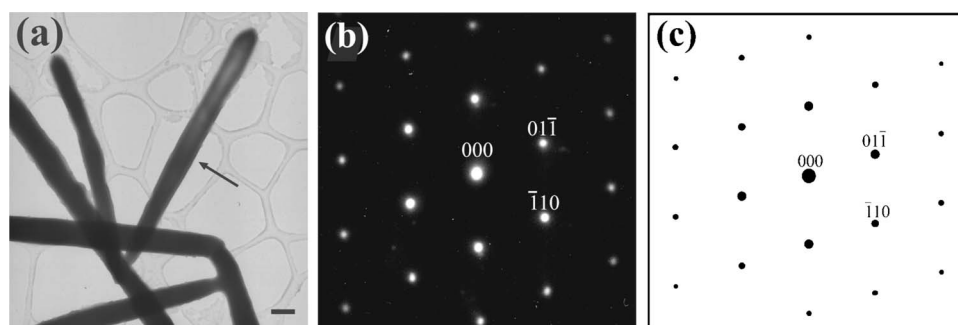


FIG. 3. (a) A group of needle-shaped wires, transferred onto a TEM grid. The scale bar denotes $500\ \text{nm}$. (b) The measured diffraction pattern of the wire segment indicated by the arrow in (a). (c) The simulated diffraction pattern of crystalline indium, observed from the $[111]$ direction.

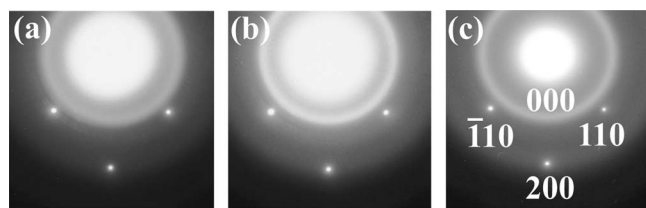


FIG. 4. The selected area diffraction patterns measured from the (a) lower third, (b) middle third, and (c) upper third of the $\sim 5\text{-}\mu\text{m}$ -long wire segment indicated by the arrow in Fig. 3(a).

same distances from the 000 spot, and no double (or multiple) sets of diffracted spots are visible. These observations indicate that this wire segment is a single-crystal domain of highly pure indium. Of 13 wire segments examined in this manner, some as long as $25\ \mu\text{m}$, the crystal structure was found to be invariant along the length of each segment, indicating that this growth procedure produces indium wire segments that are single crystals.

We determined the growth direction of the wires by comparative analysis of the selected area diffraction patterns and the corresponding real-space images. Analysis shows that eight of the nine main segments (as opposed to side-branches) examined in this study grew nearly perpendicular to the $\{110\}$ plane with up to 8° of deviation. Often, the least stable surface of a crystal grows the fastest,¹² and the $\{110\}$ plane is one of indium's high energy planes, with a surface energy merely 1% smaller than that of the $\{011\}$ plane, the highest energy surface under ultrahigh vacuum.¹³ The aqueous environment and the applied electric fields may further influence the growth direction, so it is not surprising that the wires grow predominantly in the $\langle 110 \rangle$ direction. However, determining the origin of this preference will require further study.

We observed similar dendritic growth behavior in saturated solutions of lead acetate and nickel sulfate. While a conclusive determination of the electrochemical mechanisms underlying this wire-growth phenomenon is beyond the scope of this work, the necessity that the solutions be saturated with salt suggests that supersaturation drives the dendritic solidification process,^{14,15} just as supercooling drives dendritic growth in pure materials.¹⁶ We expect our ongoing investigation into the growth mechanism to enable the di-

rected dendritic growth of crystalline wires from a broad range of materials.

This work establishes an innovative, electrochemical approach to growing single-crystal, metallic wires between targeted sites in on-chip circuitry, demonstrating the possibility of using simply prepared aqueous solutions to grow submicron wires composed of metals of choice. As the directed growth and interfacing of wires are not easily attainable with other crystal-growth techniques, such as the vapor-liquid-solid mechanism,^{17,18} this work is expected to prove useful in applications requiring the *in situ* growth of single-crystal interconnects.

This work was supported by the National Science Foundation (NER-0304413) and Oklahoma EPSCoR (EPS-132354). The authors thank Daniel R. Grischkowsky for generously sharing the cleanroom facilities used to produce the lithographic electrode arrays.

¹K. D. Hermanson, S. O. Lumsdon, J. P. Williams, E. W. Kaler, and O. D. Velev, *Science* **294**, 1082 (2001).

²B. Ozturk, I. Talukdar, and B. N. Flanders, *Appl. Phys. Lett.* **86**, 183105 (2005).

³A. Bezryadin, R. M. Westervelt, and M. Tinkham, *Appl. Phys. Lett.* **74**, 2699 (1999).

⁴J. Tang, B. Gao, H. Geng, O. D. Velev, L. C. Qin, and O. Zhou, *Adv. Mater. (Weinheim, Ger.)* **15**, 1352 (2003).

⁵R. Kretschmer and W. Fritzsche, *Langmuir* **20**, 11797 (2004).

⁶K. G. Libbrecht and V. M. Tanusheva, *Phys. Rev. Lett.* **81**, 176 (1998).

⁷C. Cheng, R. K. Gonela, Q. Gu, and D. T. Haynie, *Nano Lett.* **5**, 175 (2005).

⁸B. Ozturk, C. Blackledge, D. R. Grischkowsky, and B. N. Flanders, *Appl. Phys. Lett.* **88**, 073108 (2006).

⁹Y. Sawada, A. Dougherty, and J. P. Gollub, *Phys. Rev. Lett.* **56**, 1260 (1986).

¹⁰D. Grier, E. Ben-Jacob, R. Clarke, and L. M. Sander, *Phys. Rev. Lett.* **56**, 1264 (1986).

¹¹H. E. Swanson, R. K. Fuyat, and G. M. Ugrinic, *Natl. Bur. Stand. Circ. (U. S.)* **3**, 3 (1954).

¹²A. Zangwill, *Physics at Surfaces* (Cambridge University Press, New York, 1988).

¹³J. C. Heyraud and J. J. Métois, *Surf. Sci.* **177**, 213 (1986).

¹⁴J. S. Langer, *Rev. Mod. Phys.* **52**, 1 (1980).

¹⁵K. G. Libbrecht and V. M. Tanusheva, *Phys. Rev. E* **59**, 3253 (1999).

¹⁶M. E. Glicksman and A. O. Lupulescu, *J. Cryst. Growth* **264**, 541 (2004).

¹⁷W. G. Miao, Y. Wu, and H. P. Zhou, *J. Mater. Sci.* **32**, 1969 (1997).

¹⁸A. M. Morales and C. M. Lieber, *Science* **279**, 208 (1998).

¹⁹See EPAPS Document No.E-APPLAB-88-261622 for real-time movies of the dendritic and needle-growth-processes. This document can be reached via a direct link in the online article's HTML reference section or via the EPAPS homepage (<http://www.aip.org/pubservs/epaps.html>).